1991-03-01

# Generation of hard x-rays from transition radiation using high-density foils and moderate-energy electrons

Piestrup, M. A.

American Physical Society

Physical Review A, v. 43, no. 5, March 1, 1991, pp. 2387-2395
http://hdl.handle.net/10945/47498

# Generation of hard x rays from transition radiation using high-density foils and moderate-energy electrons

M. A. Piestrup
*Adelphi Technology Inc., 285 Hamilton Avenue, Suite 430, Palo Alto, California 94301*

M. J. Moran
*Lawrence Livermore National Laboratory, University of California, Livermore, California 94550*

D. G. Boyers and C. I. Pincus
*Adelphi Technology Inc., 285 Hamilton Avenue, Suite 430, Palo Alto, California 94301*

J. O. Kephart
*IBM T. J. Watson Research Center, Yorktown Heights, New York, 10598*

R. A. Gearhart
*Stanford Linear Accelerator Center, Stanford, California 94305*

X. K. Maruyama
*Naval Postgraduate School, Monterey, California 93943*
(Received 18 September 1990)

In experiments using targets consisting of many thin metal foils, we have demonstrated that a narrow, forward-directed cone of transition radiation in the 8- to 60-keV spectral range can be generated by electron beams with moderate energies (between 100 and 500 MeV). The theory suggests that high-density, moderate-atomic-number metals are the optimum foil materials and that the foil thickness can be chosen to maximize photon production within a desired spectral range. The three targets used in the experiments consisted of 10 foils of 1-$\mu$m-thick gold, 40 foils of 8.5-$\mu$m stainless steel, and 20 foils of 7.9-$\mu$m copper. The efficiency with which hard x rays are generated, and the fact that the requisite electron-beam energies are lower by a factor of 5 to 10, make such a radiation source an attractive alternative to synchrotron radiation for applications such as medical imaging, spectroscopy, and microscopy.

## I. INTRODUCTION

### Transition radiation as a hard-x-ray source

Transition radiation, the production of photons when energetic charged particles cross the interface between two dielectric media,[1-6] is a mechanism whose characteristics have been studied both theoretically and experimentally for a wide range of conditions. In most cases, the agreement between theory and experiment has been excellent. The ability to predict the emission distribution is limited only by our understanding of the relevant dielectric constants. A number of early experiments with ultrarelativistic electrons and periodic radiators demonstrated the spatial coherence of transition radiation.[7-10] More recently, medium-energy electrons (17–100 MeV) have generated intense transition radiation with spectra that were rich in 1- to 5-keV x rays.[11-16] Previously, such photon energies had been obtained with electron energies in the GeV range.[17] The practical application of transition radiation to a variety of problems will be greatly enhanced if the trend toward efficient generation of x rays with lower-energy electrons can be continued. The present work has shown that hard x rays can be generated efficiently with more practical electron-beam energies by using radiators consisting of multiple thin foils of high-density materials such as gold, stainless steel, or copper.[18]

Transition radiation is a bright source of x rays. The radiation produced per electron is at least two orders of magnitude greater than for synchrotron radiation. Electrons of relatively moderate energy can produce transition radiation, whereas greater currents of much higher-energy electrons are needed to produce an equivalent amount of synchrotron radiation at the same wavelength. Because of the efficiency of transition radiation production and the availability of medium-energy electron-beam sources, applications in areas such as x-ray lithography, medical imaging, and microscopy are attractive.

The research presented here was motivated primarily by the desire to produce a new source of x rays for a noninvasive method of coronary angiography based on the use of x rays at photon energies close to the $K$ edge of iodine at 33.16 keV.[19] As such, we have designed the foil stacks described here to produce peak-photon energies around 30 keV.

The present work addresses several characteristics of transition radiation generated by thin high-density foils.

 

These characterisitics include the basic intensity and energy spectrum, the relative intensity from bremsstrahlung, and the effects of elastic electron scattering in the foils. We have measured the total photon-energy spectrum of transition radiation generated by high-density foils and have found that the measured distributions match our theoretical predictions. In previous experiments we have acquired some of the first data available to demonstrate the ability of thin foils to survive relatively high continuous electron-beam currents.[20] In the paragraphs below, we will discuss the relevant theoretical descriptions and present some recent experimental results.

## II. THEORY

### A. Theoretical determination of the photon spectra

When a relativistic charged particle crosses the boundary between two different dielectric media, the interaction between the Coulomb field of the particle and the dielectric boundary generates transition radiation which, for the x-ray spectral region, is radiated into a narrow, forward-directed hollow cone. The angular distribution has a maximum at an angle of $1/\gamma$, where $\gamma$ is the relativistic energy parameter given by the total energy divided by its rest mass, and has a minimum in the direction of particle motion. The energy spectrum for a single interface is essentially "white" and extends from the microwave into the hard-x-ray spectral region, with the high-energy cutoff determined by the high-frequency limit of the dielectric interface. However, in real targets consisting of one or more single foils, with two interfaces per foil, the effects of spatial coherence, photon absorption, and electron scattering induce predictable changes in the angular and spectral distributions. Thus, the emission distribution radiated by a specific target can be tailored by careful choice of the number, thickness, spacing, and material of the foils, and by choice of particle (electrons in our case) energy. A series of experiments have shown how to choose the above parameters for the optimization of emissions in the hard-x-ray spectral region. One procedure that can be used to make these choices will be outlined below.

Forty-five years ago, Ginzburg and Frank[1] correctly predicted the differential production of transition radiation at a single interface to be given by

$$\frac{d^2N_o}{d\omega d\Omega}=\left[\frac{\alpha\omega\sin^2\theta}{16\pi^2c^2}\right](Z_1-Z_2)^2 , \tag{1}$$

where the fine-structure constant $\alpha=\frac{1}{137}$, and $Z_i$ are "formation lengths" given by[14]

$$Z_i=\frac{2\beta c}{\omega(1-\beta\sqrt{\epsilon_i-\sin^2\theta})} . \tag{2}$$

$\epsilon_i(i=1,2)$ are the permittivities of the two media, $\omega$ is the photon angular frequency, $\beta=v/c$ is the relativistic particle speed, and $c$ is the speed of light. For photons in the x-ray spectral region the permittivities generally can be approximated by $\epsilon_i=1-(\omega_i/\omega)^2$, where $\omega_i$ are the respective electron plasma frequencies ($\omega_i^2=4\pi N_e e^2/m$). This approximation generally is valid for $\omega\gg\omega_i$. The formation length can be thought of as the distance that the charged particle must travel in order to experience a phase change of $\pi$ rad with respect to a copropagating photon. For the present parameters of interest, $Z_i$ vary from 1 to 10 $\mu$m, and the plasma frequencies range from 30 to 80 eV.

The spectral photon density at an interface can be integrated over angles to give an approximate form for the spectral intensity:[17]

$$\frac{dN}{d\omega}=\left[\frac{2\alpha}{\pi\omega}\right]\left[\left[\frac{1}{2}+\frac{1}{b}\right]\ln(1+b)-1\right] , \tag{3}$$

where $b=(\gamma\omega_2/\omega)^2$, $\gamma=E/E_0$, $E$ is the electron-beam energy, $E_0=0.511$ MeV, and $\omega_2$ is the plasma frequency of the foil material. When $b\gg1$ (or $\omega\ll\gamma\omega_2$), the spectral density is proportional to $\ln\gamma$, is of the order of $\alpha/\pi\omega$, and is relatively insensitive to small changes in the particle beam energy. For moderate-energy electron beams of about 100 MeV, the spectral flux is roughly constant ($1.6\times10^{-5}$ photons/10% bandwidth) when $\omega=\gamma\omega_2$. For frequencies $\omega>\gamma\omega_2$, the emission rate declines as $(\omega_2/\omega)^4$. In general, efficient emission is restricted to frequencies $\omega<\gamma\omega_2$. Thus the frequency $\omega_c=\gamma\omega_2$ can be regarded as a "cutoff" frequency above which the radiation falls drastically. From this condition one can then determine a minimum electron energy required for x-ray emission at frequency $\omega$ given by $E=E_0\omega/\omega_2$.

To minimize the cost of construction and operation of the accelerator, one would like to keep the electron-beam energy as low as possible. This is achieved by choosing high-density foils, thus increasing the "cutoff" frequency $\omega_c=\gamma\omega_2$. But since high-density materials often have higher atomic numbers, bremsstrahlung can be large if the atomic number is too high. Hence, in some cases it is important to minimize the bremsstrahlung since it has a flat spectral power density from very long wavelengths to photon energies equal to that of the electron-beam energy. Otherwise, extremely hard x rays would be produced at high atomic number, which are detrimental to the x-ray optics and other experimental apparatus directly in line with the x-ray flux. Thus it is important to select foil materials with thickness and densities that minimize the bremsstrahlung and maximize the transition radiation. Selection of materials of high-density and moderate atomic number is therefore desirable in thse situations. For example, iron (stainless steel) and copper foils are excellent candidates since they have comparably high densities and moderate atomic numbers.

High-density foils which also have high atomic numbers such as gold or tungsten can be used if it is desirable to lower the electron-beam energy further and if extremely hard bremsstrahlung contamination of the transition radiation spectrum does not matter.

Equation (1) gives differential photon-production efficiency per electron at a single interface. The photons are spatially coherent with respect to the electron because the photons are generated at the interface. This spatial

coherence means that, in targets with multiple interfaces, interference effects between successive surfaces can change the angular and spectral photon emission distributions. In the case of a single thin foil with two surfaces, the emission distribution can be written[1-3,17,21]

$$\frac{d^2N_f}{d\omega\, d\Omega} = \left[\frac{d^2N_0}{d\omega\, d\Omega}\right] 4\sin^2\left[\frac{l_2}{Z_2}\right], \tag{4}$$

where $l_2$ is the foil thickness.

This description is generally valid for the foils that we use; but for thick high-atomic-number foils, the electrons may experience sufficient numbers of Coulomb collisions to nullify the mutual coherence of photons generated at the two surfaces. Limits on the foil thickness that can be used without nullifying the single-foil coherence will be discussed more fully in a later section. For the moment, note that the interference effects are modulated on a length scale of $Z_2$. Since $Z_2$ is usually a few microns, this means that structures with dimensions on the order of microns coherently radiate x rays with wavelengths on the order of angstroms.[8-10]

The most efficient transition radiation sources are radiators consisting of multiple foils chosen to enhance the desired photon frequencies with the available electron-beam energy. In some cases the spatial coherence of photons can extend throughout a multiple-foil radiator and can result in highly defined emission distributions.[7-10] In the present situation, however, such effects will not be resolvable. For our purposes, the total emission from a multiple-foil radiator is simply the sum of intensities generated by the individual foils, taking into account the partial absorption by "downstream" foils of the photon generated by "upstream" foils. Analysis reveals that the total emission distribution from such a radiator can be described by a modification of Eq. (4):

$$\frac{d^2N_M}{d\Omega\, d\omega} = \frac{d^2N_f}{d\Omega\, d\omega}\left[\frac{1-\exp(-M\sigma)}{1-\exp(-\sigma)}\right], \tag{5}$$

where $M$ is the number of foils in the radiator and $\sigma = l_2/l_{\rm abs}$, where $l_{\rm abs} = 1/\mu_2$ is the x-ray absorption length and $\mu_2$ is the linear absorption coefficient of the foil material.[22] When $\theta \ll 1$ and $\omega \gg \omega_i$, Eq. (5) can be written in the fairly simple approximate form:

$$\frac{d^2N}{d\Omega\, d\omega} \simeq \left[\frac{\alpha}{\omega}\right]\left[\frac{2\beta\omega_2^2}{\pi\omega^2}\right]^2\left[\frac{\sin^2(l_2/Z_2)\sin^2\theta}{[(1/\gamma)^2+\theta^2]^2[(1/\gamma)^2+\theta^2+(\omega_2/\omega)^2]^2}\right]\left[\frac{1-\exp(-M\sigma)}{1-\exp(-\sigma)}\right]. \tag{6}$$

This result has been used successfully to predict the emission distributions from sources for a wide variety of experimental conditions.[15,16]

By noting the exponential dependence on the number of foils in Eq. (6), we can achieve approximately 87% of the total possible flux by setting $M \simeq 2/\sigma = 2/\mu_2 l_2$. The absorption constant $\mu_2$ is to be evaluated at the desired frequency of emission. This value can be used to estimate the optimum number of foils.

The distribution in Eq. (6) combines three basic factors: (a) the single-surface emission modified by (b) the single-foil resonance, and (c) the alteration of this band resulting from absorption by downstream foils of photon emitted by upstream foils. When absorption by the foils is insignificant, then the single-foil resonance (phase addition of the x rays between the front-and-back surfaces of the foil) will enhance photons with wavelengths that give $l_2 \simeq (\pi/2)Z_2$. With the approximations described above and using Eq. (2), this condition can be written as

$$l_2 = \frac{\lambda}{2/\gamma^2+\omega_2^2/\omega^2}, \tag{7}$$

where we have assumed the radiator to peak at $\theta \simeq 1/\gamma$ and $\omega$ is chosen as the desired frequency of emission. The foil thickness can vary appreciably without drastic changes in the spectral shape and peak-photon production.

When absorption in a single foil is fairly small, but the net absorption by an entire radiator is significant, then absorption-induced changes in the spectrum are described by the exponential term in Eq. (6). Depending on the radiator of interest, the spectral dependence of the absorption term can result in major changes in the emission spectrum. As an example, we show in curve (a) of Fig. 1 the theoretical spectrum of the transition and bremsstrahling radiation produced by a foil stack composed of 10 foils of 1-$\mu$m-thick gold (used in the experi-

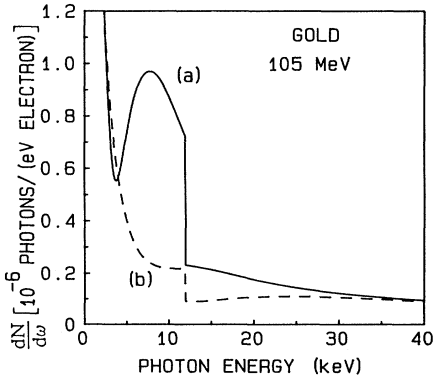


FIG. 1. Predicted spectral photon density (a) for ten foils of 1-$\mu$m gold and (b) an equivalent thickness (10-$\mu$m) single foil of gold. The electron-beam energy was 105 MeV. Parameters were chosen to match the experimental conditions given in Table I.

ment). This is compared to curve (b), which is the bremsstrahlung and front-and-back surface transition radiation from a single, equivalent-thickness (10-$\mu$m) gold foil. At the low-photon-energy end of the spectrum in curve (a), the photon flux increases with softer photon energies ($\omega < 3.5$ keV). Both the transition radiator and the equivalent-thickness single foil have this characteristic soft-x-ray rise. This is due to transition emission from the last-foil interface. As the photon energy increases, the photon flux decreases because of the decreased photon production per foil interface. The flux begins to increase again above 3.5 keV because of the rapid drop in x-ray absorption in the foils. At 13.7 keV there is a sudden drop in photon flux because of the $L$-shell photon absorption edge.

We can optimize photon production by choosing the system parameters with care. Given sufficient electron energy $E > E_0\omega_c/\omega_2$, we can make the spectrum peak at a desired frequency $\omega_p$ by choosing the foil thickness to be given by Eq. (7) with $\omega \simeq \omega_p$, and

$$M \simeq 2/\mu_2(\omega_p)l_2 \ . \tag{8}$$

This assumes that $\omega_p$ is not near the $K$ or $L$ photoabsorption edges. This optimization procedure was done for the three radiators used in the experiment.

However, the optimization procedure is not critical for optimum photon production. The foil thickness, electron-beam energy, and number of foils can vary widely without an appreciable change in the observed spectrum. The stainless-steel radiators used in this work had foil thicknesses of 8.5 $\mu$m, which were determined by commercial foil availability, whereas the calculated ideal thickness for resonance at 33 keV was 7.3 $\mu$m. In addition, the number of foils was less than $M \simeq 2/\mu_2 l_2$. The foil-stack parameters are given in Table I along with the ideal calculated values shown in parentheses.

The calculated spectra for the stainless-steel (Fe) radiator at 500 and 400 MeV and the copper (Cu) radiator at 500 MeV are given in Fig. 2. These radiators and energies were used in the experiments outlined below. The spectra all peak at approximately 30 keV, even though the foil thickness and number were not ideal.

The quasimonochromaticity of the source can be improved by filtering out the soft x rays. One can attenuate the soft x rays by placing another foil downstream of the foil stack after the beam dump so that the electrons do not strike the new foil. The new foil, composed of the same material as the foil stack, will act as a high-pass filter attenuating the soft x rays. For example, placing a 8.5-$\mu$m stainless-steel foil downstream of the steel-foil stack of Fig. 2 will result in a significant drop in x rays below 12 keV. This single foil will screen the soft x rays which originate from the last interface of the last foil. The resulting spectrum will range from 20 to 40 keV.

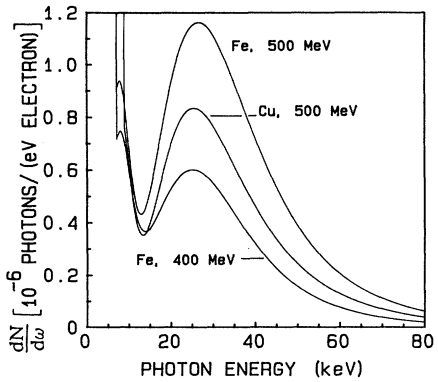


FIG. 2. Predicted spectral photon density for the stainless-steel- and copper-foil stacks used in this experiment. Parameters were chosen to match the experimental conditions given in Table I.

### B. Bremsstrahlung

A second mechanism that contributes to the photons emitted when relativistic electrons pass through thin foils is bremsstrahlung, which is generated when the electrons suffer inelastic Coulomb collisions with atoms in the solid material. For soft x rays and low-atomic-number radiators, we have found bremsstrahlung to be small compared to transition radiation.[11–16] However, for the present application, with harder x rays and higher-atomic-number radiators, bremsstrahlung can become a significant fraction of the total radiation. One description of bremsstrahlung that is appropriate for the present purposes assumes relativistic incident electrons and complete screening of the nuclear charge by atomic electrons. In this case the number of bremsstrahlung photons $N_B$ generated by an electron traversing a thickness $dl$ of radiator material can be written:[23]

TABLE I. Radiators used in experiments.

| | Peak frequency $\omega$ (keV) | Plasma frequency $\omega_2$ (eV) | Foil number $M$ | Foil thickness $l_2$ ($\mu$m) | Foil spacing $l_1$ (mm) | Electron energy $E$ (MeV) |
|---|---|---|---|---|---|---|
| Gold | 8 | 80.3 | 10 (40)[a] | 1.0 (1.05)[b] | 1.5 | 105 |
| Stainless steel | 33 | 55.1 | 40 (53) | 8.5 (7.7) | 1.5 | 500 |
| Stainless steel | 33 | 55.1 | 40 (66) | 8.5 (6.2) | 1.5 | 400 |
| Copper | 33 | 58.2 | 20 (36) | 7.8 (7.22) | 1.5 | 500 |

[a]Maximum number of foils from $M = 2/\mu_2 l_2$.
[b]Optimum foil thickness using Eq. (7) at the desired peak frequency.

$$\frac{d^2N_b}{d\omega\, d\Omega}=N_0\left[\left[\frac{8\alpha}{\pi\omega}\right]Z^2r_0^2\gamma^2\ln\left[\frac{233}{Z^{1/3}}\right]\frac{1+\gamma^4\theta^4}{1+\gamma^2\theta^2}\right]dl\ . \tag{9}$$

Here $N_0$ is the number of atoms per cm$^3$ of atomic number $Z$, and $r_0$ is the "classical" electron radius ($e^2/mc^2=2.8\times10^{-13}$ cm). This distribution peaks in the electron-beam direction and has an angular full width of about $1/\gamma$.

In some cases, the angle-integrated intensity will be more important; and for an electron penetrating a thickness $l$ of material (where $l=Ml_2$), the bremsstrahlung spectral density can be written:

$$\frac{dN_b}{d\omega}=N_0\left[\frac{16\alpha}{3\omega}\right]Z^2r_0^2\ln\left[\frac{233}{Z^{1/3}}\right]\times\left[1-\exp\left[\frac{l}{l_{\rm abs}}\right]\right]l_{\rm abs}\ . \tag{10}$$

This equation together with Eqs. (3) and (5) can be used to obtain a comparison of the relative spectral fluxes of transition radiation and bremsstrahlung from a multiple-foil target. When absorption by a single foil is small, the exponential term in Eq. (5) is approximately $M$, while the corresponding term in Eq. (10) is approximately $Ml_2$. In this approximation, we obtain for the ratio of transition radiation to bremsstrahlung:

$$\left[\frac{dN_t}{d\omega}\right]\Big/\left[\frac{dN_b}{d\omega}\right]\simeq\frac{1}{16N_0Z^2r_0^2l_2}\ . \tag{11}$$

Here, the factor of $l_2$ indicates that the transition-to-bremsstrahlung ratio is determined mainly by the last foil in the target. The ratio can vary widely for different situations: For 1-$\mu$m Al foils the ratio for 1-keV photons becomes about 783; but with 8-$\mu$m Cu foils the ratio for 10-keV photons becomes about 15.

The ratio in Eq. (11) is not a precise result, but is only intended to be used as an indicator of the potential for undesireable high-bremsstrahlung contributions to the total photon yield from a target. If the ratio is not large, then details of the emissions for both transition and bremsstrahlung must be considered. In this case both the angular and spectral distributions must be considered for their impact on the potential application.

### C. Elastic scattering

Another process that should be mentioned is elastic scattering of the electrons as they pass through the foil target. Although the energy lost by electrons almost always will be negligible, the transverse component introduces angular broadening of the electron beam that can change the angular distribution of emitted photons. The key parameter here is the characteristic angle $1/\gamma$. If the scattering induces angular broadening $\Delta\theta_S$, which is small compared to $1/\gamma$, then the photon distribution will have only small deviations from the ideal ones described above. However, if $\Delta\theta_S\geq1/\gamma$, then the photon distribution must be integrated over the angular distribution of electrons.

Theories describing he angular distribution associated with elastic scattering have been described previously.[24] For the present purposes it will be adequate to establish a criterion for determining when elastic becomes important, i.e., when the mean scattering angle becomes $1/\gamma$. From the Highland description we find that $\Delta\theta_S=1/\gamma$ for a total foil thickness:[25]

$$\frac{L_1}{\gamma}\simeq10^{-3}L_R\ , \tag{12}$$

where $L_R$ is the radiation length in the material of interest. For aluminum this gives $L_1/\gamma\simeq90$ $\mu$m, a total thickness that would not be useful as a high-intensity x-ray source, but for copper gives $L_1/\gamma\simeq15$ $\mu$m, a thickness that clearly is significant for the hard x-ray sources being discussed here. The broadening is not necessarily detrimental to the photon source because it could be used to "fill in" the narrow on-axis minimum of a transition radiation angular distribution. If the parameters are chosen carefully, the final distribution could be a relatively uniform cone with a half-angle of $2/\gamma$.

## III. EXPERIMENTAL RESULTS

### A. Accelerator selection

Two experiments were performed: one at the Naval Postgraduate School (NPS) Linac in Monterey, California, and one at the Stanford Linear Accelerator Center's (SLAC) test beam. The two accelerators offered a wide energy selection. The NPS linac and SLAC test beamline both offered low currents for pulse-height analysis of the transition radiation spectrum. The SLAC test beam has energies of 300 MeV to 10 GeV, useful for generating hard x rays of 30 keV or larger.

### B. The 105-MeV experiment

This experiment was performed to show that hard x rays could be obtained from a moderate-energy electron beam of only 105 MeV. The electron beam was generated using the NPS Linac in Monterey, California. The experimental apparatus is shown in Fig. 3. Electrons en-

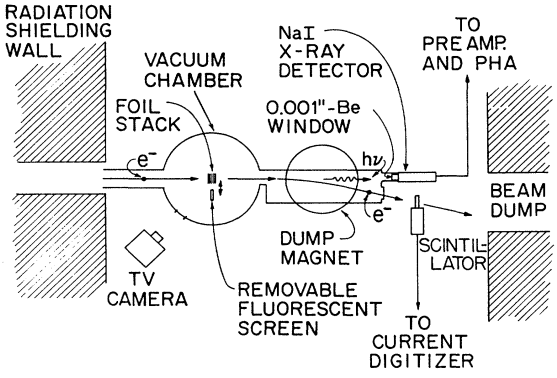


FIG. 3. Diagram of the experimental apparatus to measure hard x rays from a 105-MeV electron beam. The distance between the foil stack and the x-ray detector window is 129 cm. Ten 1-$\mu$m gold foils were used to produce x rays from 8 to 35 keV.

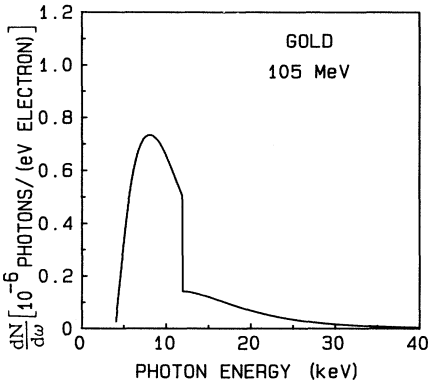


FIG. 4. Predicted spectral photon density of the difference spectrum for ten foils of 1-$\mu$m gold. Spectrum was obtained by subtracting curve (b) from curve (a) in Fig. 1.

tered from the left into a vacuum chamber where they passed through the foil stack and then through a dump magnet to be deflected out of the path of the NaI detector. The x rays traveled in a $10^{-6}$-Torr vacuum before they escaped through a 12.5-$\mu$m kapton window into the air, where they were immediately captured by a NaI detector. The detector consisted of a 1-mm-thick NaI crystal with a 25.4-$\mu$m beryllium window and photomultiplier. The detector's peak sensitivity is at 50 keV, and its useful bandwidth, as stated by the manufacturer, is from 4 to 100 keV. Data was gated with the electron-beam spill to reduce the noise background. The electron-beam current was not measured, but the total charge was monitored and kept constant between measurements. At the beginning and end of the experiments, a 5894-eV $Fe^{55}$ x-ray source was used to calibrate the spectra. The detector drift was less than 5% throughout the whole experiment.

The target measured during this experiment was 10 foils of 1-$\mu$m-thick gold. These thin foils were mounted on 1.5-mm stainless-steel spacers in order to maintain adequate support. Since multiple scattering of the electrons was large, no attempt was made to achieve resonance effects between foils (the condition where there is in-phase addition from one foil to another).

In processing the experimental data, we account for the bremsstrahlung and other spurious ionizing radiation from the accelerator by subtracting the single-foil data from the foil-stack data, resulting in a difference spectrum. Unfortunately this also eliminates the back surface transition radiation (TR) from the last (downstream) foil. As we can see from the gold-foil-stack example of Fig. 1(a), the x rays generated by the last-foil interface are quite important at soft-x-ray energies. The difference spectrum can thus be characterized by the following expression: multiple-foil TR plus bremsstrahlung plus spurious radiation minus the sum of bremsstrahlung and front-and-back surface TR and spurious radiation equals the difference spectrum. The calculated difference spectrum of Fig. 4 lacks the single-interface TR but it gives a somewhat clearer picture of the hard-x-ray spectrum, especially when spurious radiation sources (e.g., collimators, irises) are upstream of the transition radiator.

Measured spectra from the 10-foil transition radiator and the 10-$\mu$m foil (background) are compared in Fig. 5. The measured ratio of transition radiation to background was 2:1 at the radiation peak. The measurements were made for the same amount of total charge passing

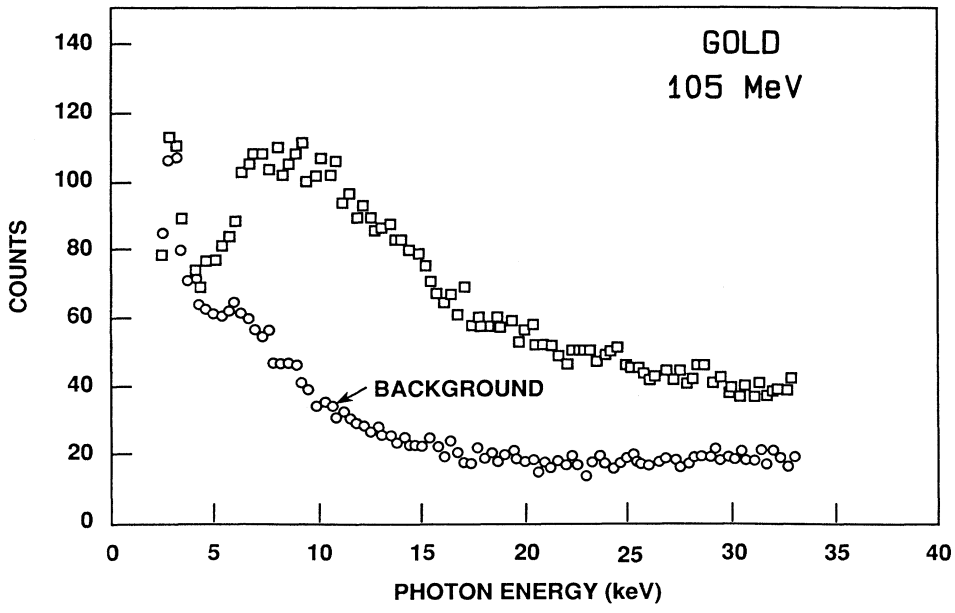


FIG. 5. The measured number of counts for ten 1-$\mu$m gold foils. The electron-beam energy was 105 MeV. The background emission from a single foil is also shown. The background emission is composed of front-and-back surface transition radiation, bremsstrahlung, and other ionizing radiation originating from upstream of the foil stack and from the close proximity to the beam dump.

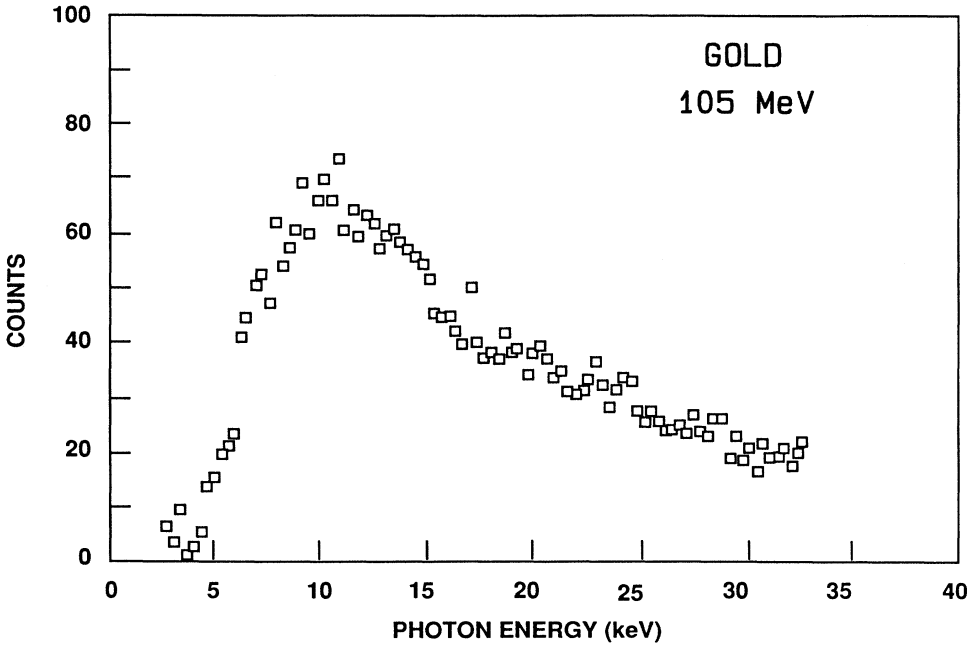


FIG. 6. The relative number of counts from a transition radiator with the background subtracted. The electron-beam energy was 105 MeV and the radiator was ten 1-$\mu$m foils of gold.

through each target, but the absolute amount of charge was not measured.

Figure 6 shows the difference spectrum, which is to be compared with the calculated spectrum shown in Fig. 4. The peak has an apparent shift to harder photon energies from 7 to 10 keV. This may be due to the uncertainty of the subtracted spectrum at the lower photon energies due to the large amount of spurious radiation and the low number of counts per channel.

### C. The 400- and 500-MeV experiments

The spectral photon density of the radiation from a 400- and 500-MeV electron beam was measured at SLAC using the apparatus diagrammed in Fig. 7. Electrons emerged from a beam pipe passing through the foil stack and then through a deflection magnet to be deflected out of the path of the NaI detector. The detector is the same as was used in the Monterey experiments. The data was gated with the electron-beam spill. The x rays traveled entirely in helium before reaching the detector. At the beginning and end of the experiments, $Fe^{55}$ and $Am^{241}$ sources were used to calibrate the spectra, and the detector drift was less than 1% throughout the whole experiment. Current pulses were monitored using a scintillator just before the beam dump so that the total charge could be kept constant for all runs.

The absolute current was measured by reducing the number of electrons so that the count rate at the scintillator was less than 0.2 photons per pulse (adequate statistics for counting with a scintillator). The peak current at the test-beam target that was upstream of the experiment was then noted. The current was then increased so that adequate numbers of photons were obtained. By assuming that there was a linear relationship between the current at the test beam and the final number of electrons at the foil stack, the total number of electrons passing through the experiment could be estimated. For example, at 500 MeV the total number of electrons to achieve an adequate photon count of 0.2 photons per pulse was approximately 5 electrons per pulse. However, the number of electrons varied between 3 to 7 electrons per pulse during collection for each transition target. At higher rates this could result in pulse pileup skewing the spectrum to harder-x-ray frequencies.

The stainless-steel-foil stack was mounted on 3.2-mm-thick aluminum rings with an inside diameter of 3.8 cm. The copper foils were mounted on 1.5-mm stainless-steel spacers with an inside diameter of 1 cm. As in the previous experiment, no attempt was made to achieve reso-

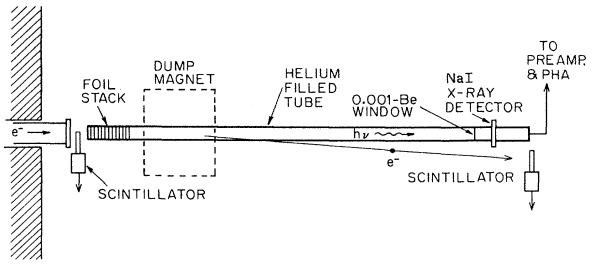


FIG. 7. Diagram of the experimental apparatus to measure the hard-x-ray flux from 20 7.9-$\mu$m copper foils and 40 8.5-$\mu$m foils of stainless steel. Not shown in the diagram are two steel collimators spaced 3 m apart and just upstream of the foil stack which produced large amounts of background radiation.

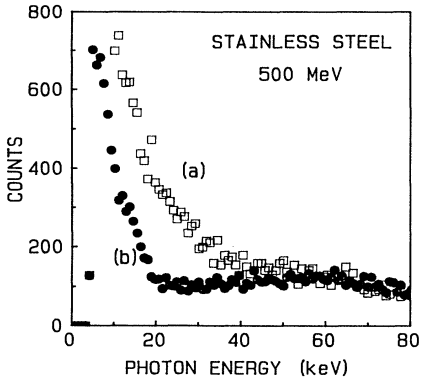


FIG. 8. The background with (b) and without (a) the single 250-$\mu$m stainless-steel foil present. The electron-beam energy was 500 MeV. With foil present, the background was attenuated at softer photon energies, indicating that the main component of background radiation came from upstream of the foils and not from the bremsstrahlung in the foils themselves.

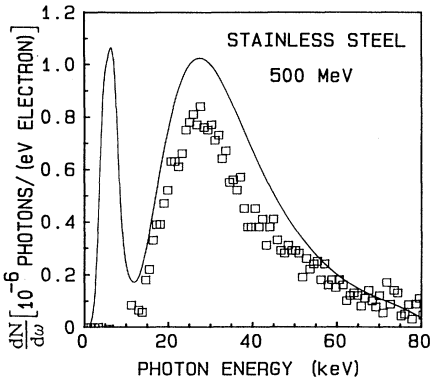


FIG. 10. The measured spectral photon density from 40 foils of 8.5-$\mu$m stainless steel at 500 MeV with the background subtracted. The calculated difference spectrum is shown for comparison. The bremsstrahlung and front-and-back surface transition radiation have been subtracted out.

nance between interfaces, since multiple scattering of the electrons was large.

As in the case of the gold foil stack, to account for the background radiation, single foils of 250-$\mu$m copper and stainless steel were used. Since these single foils were not exactly equivalent in thickness to the foil stacks, the flux from the single foil was adjusted in the data analysis so that emission from the foil and the stack could be compared. The adjusted radiation from the single foil was then subtracted from that produced by the foil stack. The background radiation was also measured with neither the stack nor the single foil present. The background with and without the single-foil 250-$\mu$m stainless-steel foil present is shown in Fig. 8. When the foil was out, there was more radiation in the soft-x-ray region than when it was inserted; thus, one must conclude that the main component of the background flux came from radiation generated upstream of the foil, and that the foil appears only to be blocking the upstream component at the softer-x-ray energies.

The background radiation was probably due to two steel collimators spaced 3 m apart just upstream of the experiment. Fortunately, transition radiation for both the copper and stainless-steel stacks was two to three times larger than that of the background and was easily seen. Thus subtraction of the background from the foil stack and the single foil gave a good estimate of the total transition radiation for hard-x-ray energies.

The number of counts from the single 250-$\mu$m foil and from 40 8.5-$\mu$m stainless-steel foils is presented in Fig. 9. The electron-beam energy was 500 MeV. In Fig. 10 the experimental difference spectrum is compared with the

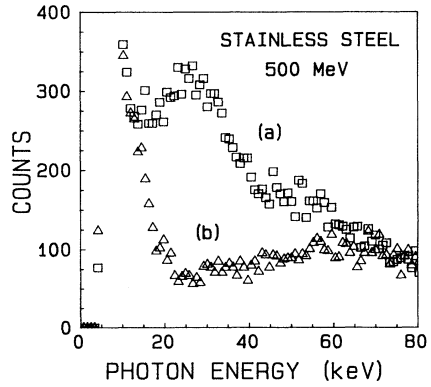


FIG. 9. The measured pulse-height count from 40 foils of 8.5-$\mu$m-thick stainless steel, curve (a). The electron-beam energy was 500 MeV. The background was produced by a single 250-$\mu$m stainless-steel foil, curve (b). The total charge through the single foil was adjusted so that emission from the foil and the stack could be compared.

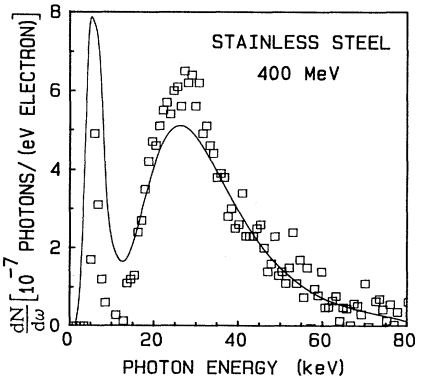


FIG. 11. The measured spectral photon density from 40 foils of 8.5-$\mu$m stainless steel at 400 MeV with the background subtracted. The calculated difference spectrum is shown for comparison. The bremsstrahlung and front-and-back surface transition radiation have been subtracted out.

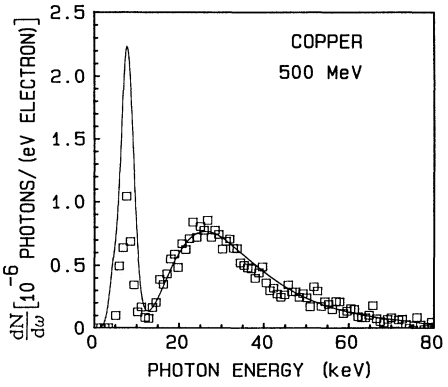


FIG. 12. The measured spectral photon density from 20 foils of 7.8-$\mu$m copper at 500 MeV with the background subtracted. The measured spectrum has been multiplied by a factor of 1.8 in order to match the calculated difference spectrum. The bremsstrahlung and front-and-back surface transition radiation have been subtracted out.

theoretical difference spectrum, which is calculated from Eq. (6) and includes the effect of the bandwidth of the detector. The bremsstrahlung and front-and-back surface transition radiation have been subtracted out, as was done for the case of gold in Fig. 2. Knowing the absolute magnitude of the charge that produced the flux, we can compare the numbers of photons per unit bandwidth per electron on an absolute scale.

Although the spectrum does not match the predicted one exactly, the agreement is probably within experimental error. As mentioned earlier, error was probably introduced by the inaccurate determination of the total charge passing through the radiator. Variations in beam current of 50% or more during the course of photon collection resulted in ratios of photon counts to beam pulses of greater than 0.2, resulting in some pileup of photon counts. The number of electrons per beam pulse varied from 10 to 100 electrons.

The rapid change in the absorption at the $K$-shell photoabsorption edge is masked by the upstream spurious radiation from the upstream collimators. At 400 MeV, a reduction of the upstream spurious radiation permitted the $K$-edge peak to be visible, if somewhat attenuated. This is shown in Fig. 11, where the same stainless-steel radiator was again used. The spectrum at harder photon energies is quite close to the predicted values.

The spectrum from a second target composed of 20 foils of 7.8-$\mu$m copper was obtained using the 500-MeV electron beam and is shown in Fig. 12. The total photon production was found to be a factor of 1.8 less than the predicted value. In order for the differential photon flux to match the predicted values, the experimental values were increased by a factor of 1.8 (shown in Fig. 11). As in the data presented in Fig. 8, the error was probably due to the variation in the beam current throughout the data collection, resulting in an inaccurate total charge measurement. Since good agreement between theory and experiment was obtained for the stainless-steal stack at 400 MeV, the disagreement for the copper stack was most likely experimental error and not due to theoretical modeling.

## IV. CONCLUSIONS

Our experiments indicate that a multiple-foil transition radiator placed in a high-current electron beam of moderate energy (100 to 500 MeV) may be an intense source of x rays. The electron-beam energy of a transition radiator is five to ten times less than that needed to produce x rays of equivalent photon energy from a synchrotron radiator. The spectral power density from the stainless-steel stack of Fig. 10 would be approximately 5 mW/keV at 30 keV for a 500-MeV, 100-$\mu$A-average current beam. Without optics, this power could be delivered to a 2.4-cm-diam annular spot 6 m from the radiator. Average currents as high as 44 $\mu$A have been sent through thin-aluminum-foil transition radiators for several hours without damage to the foils.[20] Thus average powers on the order of mW/keV and peak powers on the order of W/keV seem possible. As suggested by theoretical considerations, these experiments show that materials of high density and moderate atomic number make excellent radiators of transition radiation. High-density foils such as gold can also be used, but will produce a larger amount of bremsstrahlung. Transition radiation could serve as a relatively inexpensive source for medical imaging, spectroscopy, and microscopy.

## ACKNOWLEDGMENTS

This work was financed by the National Science Foundation of the Small Business Innovative Research (SBIR) program, Grant No. PHY-8460914. The services of linac operator Don Snyder at the Naval Postgraduate School linac are gratefully acknowledged.

[1]V. L. Ginzburg and I. M. Frank, J. Phys. (Moscow) **9**, 353 (1945).
[2]G. M. Garibyan, Zh. Eksp. Teor. Fiz. **33**, 1403 (1958) [Sov. Phys.—JETP **6**, 1079 (1958)].
[3]M. L. Ter-Mikaelian, Nucl. Phys. **24**, 43 (1961).
[4]A. I. Alikhanyan, F. R. Arutyanyan, K. A. Ispiryan, and M. L. Ter-Mikaelian, Zh. Eksp. Teor. Fiz. **41**, 2002 (1961) [Sov. Phys.—JETP **14**, 1421 (1962)].
[5]L. C. L. Yuan, C. L. Wang, H. Uto, and S. Prunseter, Phys. Rev. Lett. **31B**, 603 (1970).
[6]A. I. Alikhanian, S. A. Kankanian, A. G. Oganessian, and A. G. Tamania, Phys. Rev. Lett. **30**, 109 (1973).
[7]M. L. Cherry, D. Muller, and T. A. Prince, Nucl. Instrum. Methods **115**, 141 (1974).
[8]C. W. Fabjan and W. Struczinski, Phys. Lett. **57B**, 483 (1975).
[9]M. J. Moran, B. A. Dahling, P. J. Ebert, M. A. Piestrup, B. L. Berman, and J. O. Kephart, Phys. Rev. Lett. **57**, 1223 (1986).
[10]M. A. Piestrup, D. G. Boyers, C. I. Pincus, Qiang Li, M. J.

Moran, J. C. Bergstrom, H. S. Caplan, R. M. Silzer, D. M. Skopic, X. K. Maruyama, F. R. Buskirk, J. R. Neighbours, and G. B. Rothbart, Nucl. Instrum. Methods B **40/41**, 965 (1989).

[11]A. N. Chu, M. A. Piestrup, T. W. Barbee, Jr., R. H. Pantell, and F. R. Buskirk, Rev. Sci. Instrum. **51**, 597 (1980).

[12]A. N. Chu, M. A. Piestrup, R. H. Pantell, and F. R. Buskirk, J. Appl. Phys. **52**, 22 (1981).

[13]A. N. Chu, M. A. Piestrup, T. W. Barbee, Jr., and R. H. Pantell, J.Appl. Phys. **51**, 1290 (1980).

[14]M. A. Piestrup, P. F. Finman, A. N. Chu, T. W. Barbee, Jr., R. H. Pantell, G. A. Gearhart, and F. R. Buskirk, IEEE J. Quantum Electron. **E-19**, 1771 (1983).

[15]P. J. Ebert, M. J. Moran, B. A. Dahling, B. L. Berman, M. A. Piestrup, J. O. Kephart, H. Park, R. K. Klein, and R. H. Pantell, Phys. Rev. Lett. **54**, 893 (1985).

[16]M. A. Piestrup, J. O. Kephart, H. Park, R. K. Klein, R. H. Pantell, P. J. Ebert, M. J. Moran, B. A. Dahling, and B. L. Berman, Phys. Rev. A **32**, 917 (1985).

[17]M. L. Cherry, G. Hartmen, D. Muller, and T. A. Prince, Phys. Rev. D **10**, 3594 (1974).

[18]M. A. Piestrup, U. S. Patent No. 4,763,344 (1988).

[19]E. Rubenstein, R. Hofstadter, H. D. Zeman, A. C. Thompson, J. N. Otis, G. S. Brown, J. C. Giacomini, H. J. Gordon, R. S. Kernoff, D. C. Harrison, and W. Thomlinson, Proc. Natl. Acad. Sci. U.S.A. **83**, 9224 (1986).

[20]M. A. Piestrup and M. J. Moran, Appl. Phys. Lett. **50**, 1421 (1990).

[21]M. L. Ter-Mikaelian, *High Energy Electromagnetic Processes in Condensed Media* (Wiley-Interscience, New York, 1972), Chaps. 4 and 5 and related bibliography.

[22]E. F. Plechaty, D. E. Cullen, and R. J. Howerton, Lawrence Livermore National Laboratory, Report No. UCRL-50400, Vol. 6, Rev. 3, 1981 (unpublished).

[23]J. D. Jackson, *Classical Electrodynamics* (Wiley, New York, 1962).

[24]G. M. Garibyan, L. A. Gerorgyan, and C. Yang, Zh. Eksp. Teor. Fiz. **66**, 552 (1974) [Sov. Phys.—JETP **39**, 265 (1974)].

[25]V. L. Highland, Nucl. Instrum. Methods **129**, 497 (1975).